Seminario di passaggio al terzo anno di dottorato in Fisica degli Acceleratori

Alessandro Curcio

Supervisors: D. Giulietti and M. Petrarca

Sapienza Universita' di Roma

Roma, Ottobre 2016

Summary

Introduction

Laser-solid target interaction

Betatron Radiation: transverse emittance measurement

Relativistic Self Focusing

X-ray production from plasma filaments in front of solid targets

Self-phase modulation

Laser-plasma interaction in capillary waveguides

Resonant betatron oscillations

Laser-plasma interaction for acceleration and radiation

The Ph.D. activity of the candidate Alessandro Curcio was developed at the National Laboratories of Frascati (LNF) of the INFN and it was focused on the interaction of high-power lasers with plasmas both from a theoretical and experimental point of view. The interaction of ultra-short, high-power lasers with plasmas paves the way to novel schemes for the design of compact accelerators and $X - \gamma$ ray secondary sources.

List of main publications

⋆ *R. Pompili, M. P. Anania, F. Bisesto, M. Botton, M. Castellano, E. Chiadroni, A. Cianchi, A. Curcio, M. Ferrario, M. Galletti, Z. Henis, M. Petrarca, E. Schleifer & A. Zigler. Femtosecond dynamics of energetic electrons in high intensity laser-matter interactions. Sci. Rep. 6, 35000; doi: 10.1038/srep35000 (2016).*

⋆ *Curcio, A. et al. Trace space reconstruction of low emittance electron beams through betatron1 radiation in laser plasma accelerators. Submitted to Physical Review Letters.*

⋆ *Curcio, A. et al. Ray optics hamiltonian approach to relativistic self focusing of ultraintense lasers in underdense plasmas. To be submitted to Optics Letters.*

⋆ *Curcio, A. et al. Characterization of X-ray radiation from solid Sn target irradiated by femtosecond laser pulses in the presence of air plasma sparks. Laser and Particle Beams (2016), 34, 533538. Cambridge University Press, 2016 0263-0346/16 doi:10.1017/S0263034616000458.*

⋆*Giulietti, D. and Curcio, A. Self-Phase Modulation Effects as Laser Produced Plasma Diagnostics. Journal of Instrumentation 11(08):C08011-C08011 August 2016 DOI: 10.1088/1748-0221/11/08/C08011*

⋆ *Curcio, A. et al. Numerical and analytical models to study the laser-driven plasma perturbation in a dielectric gas-filled capillary waveguide. Op. Lett. 41, 18; http://dx.doi.org/10.1364/OL.99.099999 (2016).*

⋆ *Curcio, A. et al.Tuning of Betatron Radiation in Laser-Plasma Accelerators via Multimodal Laser Propagation through Capillary Waveguides. To be submitted to Physics of Plasmas.*

⋆ *Curcio, A. et al. Resonant interaction between laser and electrons undergoing betatron oscillations in the bubble regime. J. Plasma Phys. (2015), vol. 81, 495810513 c Cambridge University Press 2015 doi:10.1017/S0022377815000926*

Laser-solid target interaction

⋆ *R. Pompili, M. P. Anania, F. Bisesto, M. Botton, M. Castellano, E. Chiadroni, A. Cianchi, A. Curcio, M. Ferrario, M. Galletti, Z. Henis, M. Petrarca, E. Schleifer & A. Zigler. Femtosecond dynamics of energetic electrons in high intensity laser-matter interactions. Sci. Rep. 6, 35000; doi: 10.1038/srep35000 (2016).*

Electron acceleration by laser-solid target interaction/1

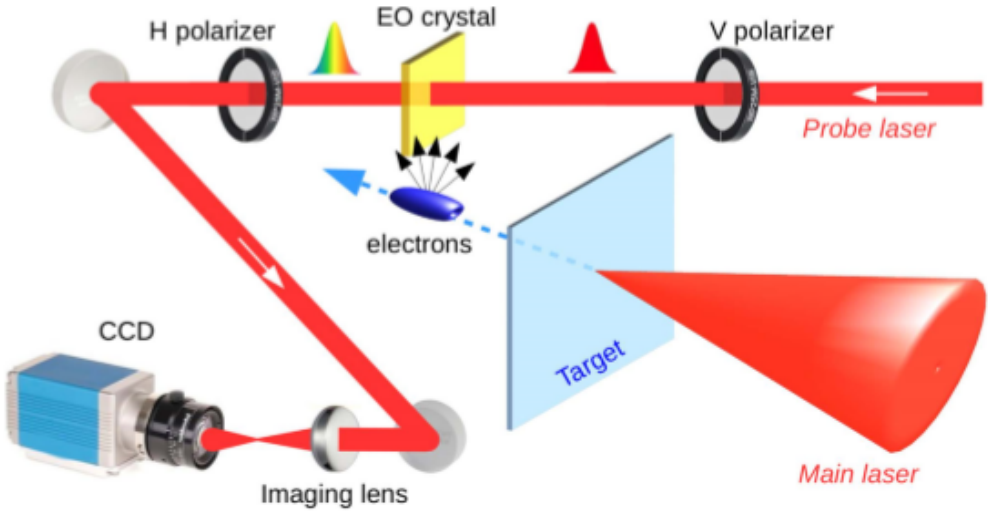

Figure: Sketch of the experiment. An f/10 parabola focuses the main laser on a metallic target ejecting a cloud of energetic electrons. An electro-optic crystal (ZnTe) is located 1 mm downstream the target. The Coulomb fields of the moving electrons optically modify the crystal, making it birefringent. This changing is temporally encoded by a linearly polarized probe laser. By measuring the polarization modulation of the probe laser, the main properties of the emitted electrons (charge, energy, temporal profile) are retrieved.

Electron acceleration by laser-solid target interaction/2

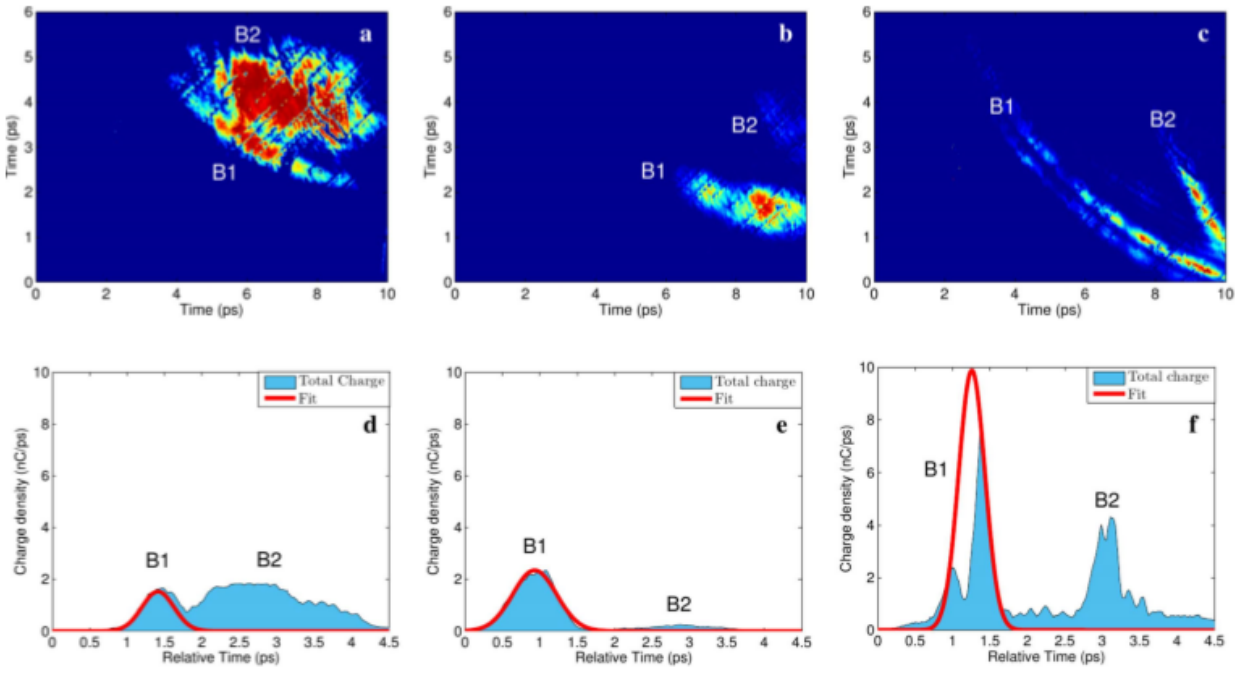

Figure: Snapshots with different target shapes. Signatures of the escaping electrons from (a) planar, (b) wedged and (c) tipped targets. The emitted charges are, respectively, (a) 1.2 nC (B1) and 3 nC (B2); (b) 2 nC (B1) and 0.3 nC (B2); (c) 7 nC (B1) and 3 nC (B2). The gaussian envelopes represent the extrapolated charge profiles of each bunch. (df) Corresponding longitudinal charge profiles. A 10^2 neutral density filter has been used in (b,c) to avoid saturation of the CCD camera.

Betatron Radiation: transverse emittance measurement

⋆ *Curcio, A. et al. Trace space reconstruction of low emittance electron beams through betatron1 radiation in laser plasma accelerators. Submitted to Physical Review Letters.*

Laser wakefield acceleration

Linear/Quasi linear regime

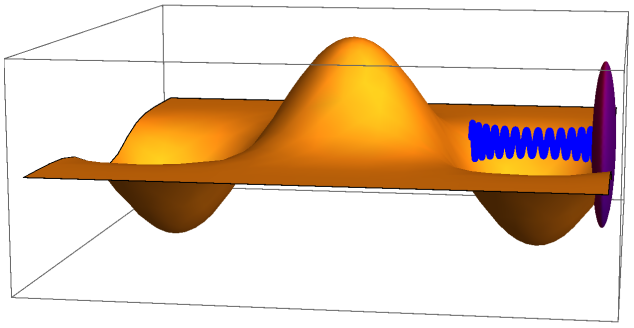

Plasma Wakefields:

$$E_z(r,\zeta) = \frac{\sqrt{\pi}}{4} a_0^2 k_p c\tau_0 E_0 \exp\left[\frac{2r^2}{w_0^2} - \frac{k_p^2 c^2 \tau_0^2}{4}\right] \cos k_p\zeta$$

$$E_r(r,\zeta) = -\sqrt{\pi} a_0^2 \frac{c\tau_0 r}{w_0^2} E_0 \exp\left[\frac{2r^2}{w_0^2} - \frac{k_p^2 c^2 \tau_0^2}{4}\right] \sin k_p\zeta$$

Bubble regime

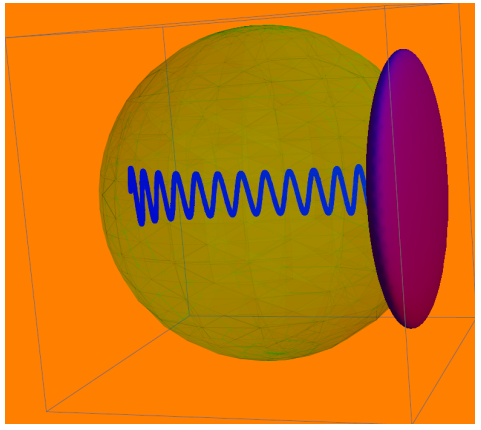

Plasma Wakefields:

$$E_z(r,\zeta) = \frac{m}{3e}\omega_p^2 \zeta \cos k_p\zeta$$

$$E_r(r,\zeta) = \frac{m}{3e}\omega_p^2 r \sin k_p\zeta$$

Characteristics of the Betatron Radiation: wiggler analogy

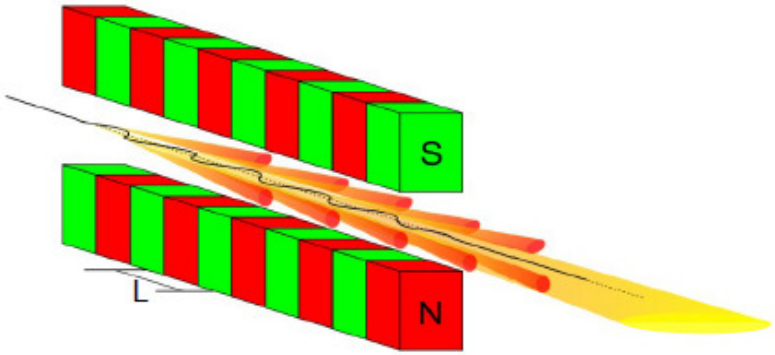

The difference between a wiggler and an undulator resides in the anharmonic motion of the oscillating particles, due to high transverse velocities, which mirrors in a broadband spectrum, while the spectrum of an undulator is narrowband.

Wiggler parameters:

$$\lambda_W = \frac{L}{2\gamma_0^2}\left(1 + \frac{K_W^2}{2} + \gamma_0^2\theta^2\right)$$

$$K_W = 0.934 B[T] L[cm]$$

$$E_c = 3\gamma_0^2 K_W \hbar\omega_W$$

Plasma wiggler parameters:

$$\lambda_b = \frac{\lambda_\beta}{2\gamma^2}\left(1 + \frac{K^2}{2} + \gamma^2\theta^2\right)$$

$$K = \gamma k_\beta r_0$$

$$E_c = 3\gamma_0^2 K \hbar\omega_b$$

A method to measure the transverse emittance: Definitions/1

$$\sqrt{\langle \Delta r^2 \rangle \langle \Delta \theta_d^2 \rangle - \langle \Delta r \Delta \theta_d \rangle^2}$$

Def. geometric emittance

$P(r)$

Transverse beam profile

$\Theta(\theta_d)$

Distribution of the angles with respect to the acceleration axis

$$\theta_d = \sqrt{\frac{\sqrt{1+\frac{1}{2}\gamma_0^2 r_\beta^2 k_{\beta 0}^2}}{4\gamma_0}} r_\beta k_p$$
$$\rightarrow \mathrm{r}_\beta(\theta_d),\ r = r_\beta/\sqrt{2}$$

Correlation function

$R(r) = rP(r)$

Distribution of the oscillation amplitudes

A method to measure the transverse emittance: Definitions/2

$S_{\gamma,r_\beta}(E,\Omega)$ Single particle spectrum

$S(E) = \int dr_\beta d\gamma R(r_\beta)\Gamma(\gamma)d\Omega S_{\gamma,r_\beta}(E,\Omega)$ Electron bunch spectrum

$\int dr_\beta R(r_\beta) \sim \sum_i R_i$ Trick

$S(E_j) \equiv S_j = \sum_i R_i S_{ij}$ Spectrum discretization

$S_{ij} = \int\int d\Omega d\gamma \Gamma(\gamma) S_{\gamma,r_{\beta,i}}(E_j,\Omega)$ Def. of the S matrix

$$S_j - \Sigma_j = \sum_{ij} R_i S_{ij} - \Sigma_j = 0$$

From the profile to the divergence

$$\omega_\beta = \omega_p/\sqrt{2\gamma}$$

Betatron frequency

$$\theta_d = \sqrt{\left\langle \left(\frac{dr}{dz}\right)^2 \right\rangle - \left\langle \left(\frac{dr}{dz}\right) \right\rangle^2} = \frac{\sqrt{2}}{2} r_\beta k_\beta$$

Single particle divergence

$$\gamma \sim \gamma_0$$

Linear correlation $\rightarrow$ zero emittance

$$\gamma^* \sim \gamma_0/\sqrt{1 + K_{\beta 0}^2/2}$$

Non linear correlation $\rightarrow$ non-zero emittance

$$\Theta(\theta_d) \propto P(r(\theta_d))$$

Distribution of the correlated divergences

Experimental Results: Setup

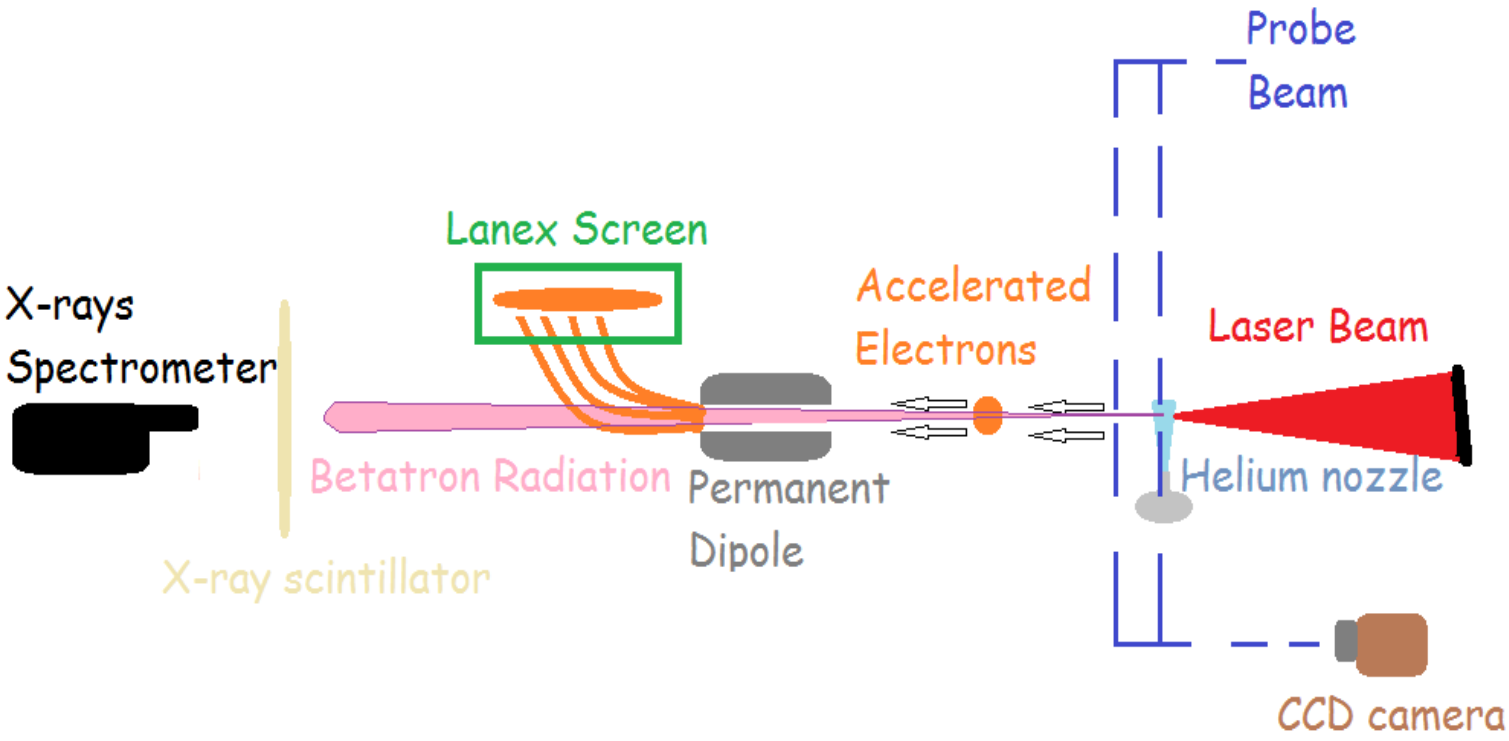

Figure: The main laser beam impinges on the supersonic helium jet, ionizing, channeling and generating plasma wakefields. The electrons, while accelerating, emit X-ray betatron radiation in the forward direction, detected by a CCD-X camera. The plasma channel is probed with interferometry. The electrons are damped out on the screen of the magnetic spectrometer.

Experimental Results: Betatron Spectrum

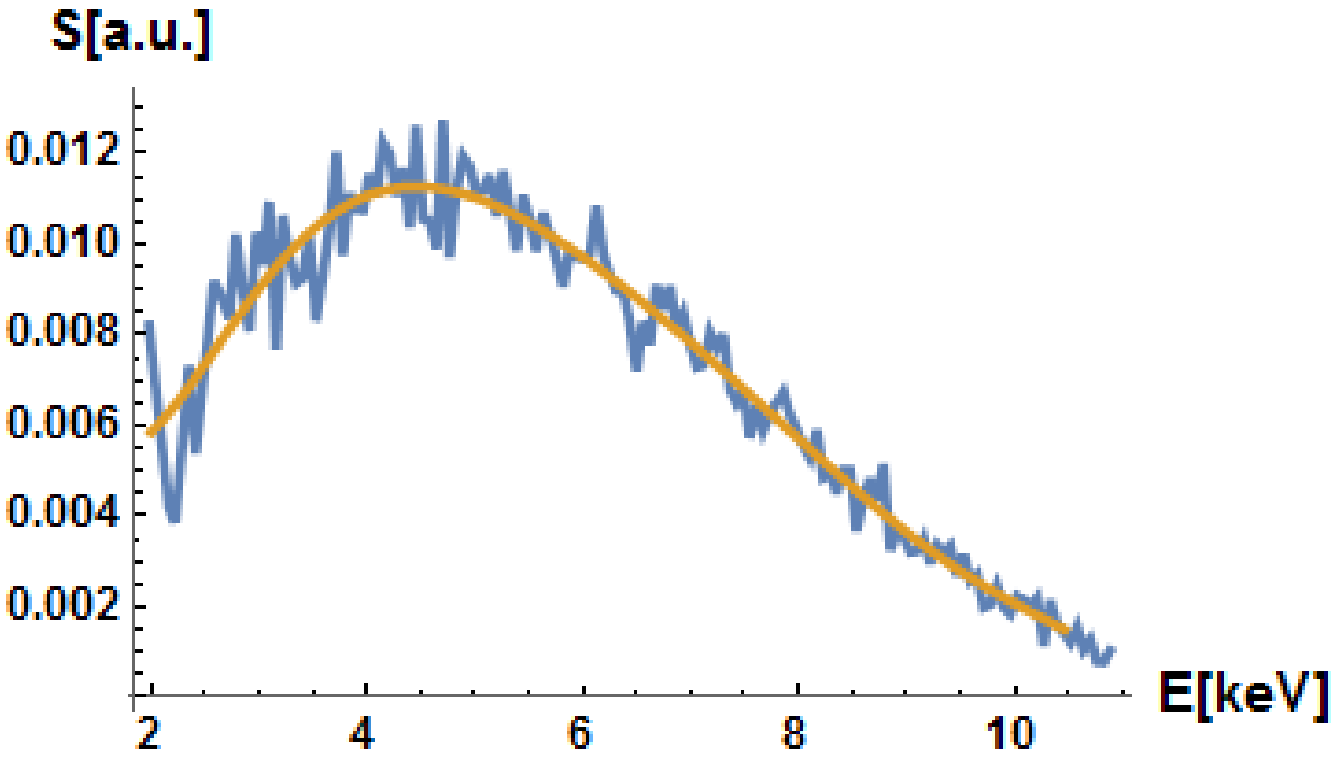

Figure: Betatron spectrum detected with a CCD-X camera working in single photon counting mode together with a polynomial fit.

Experimental Results: Electron Spectrum

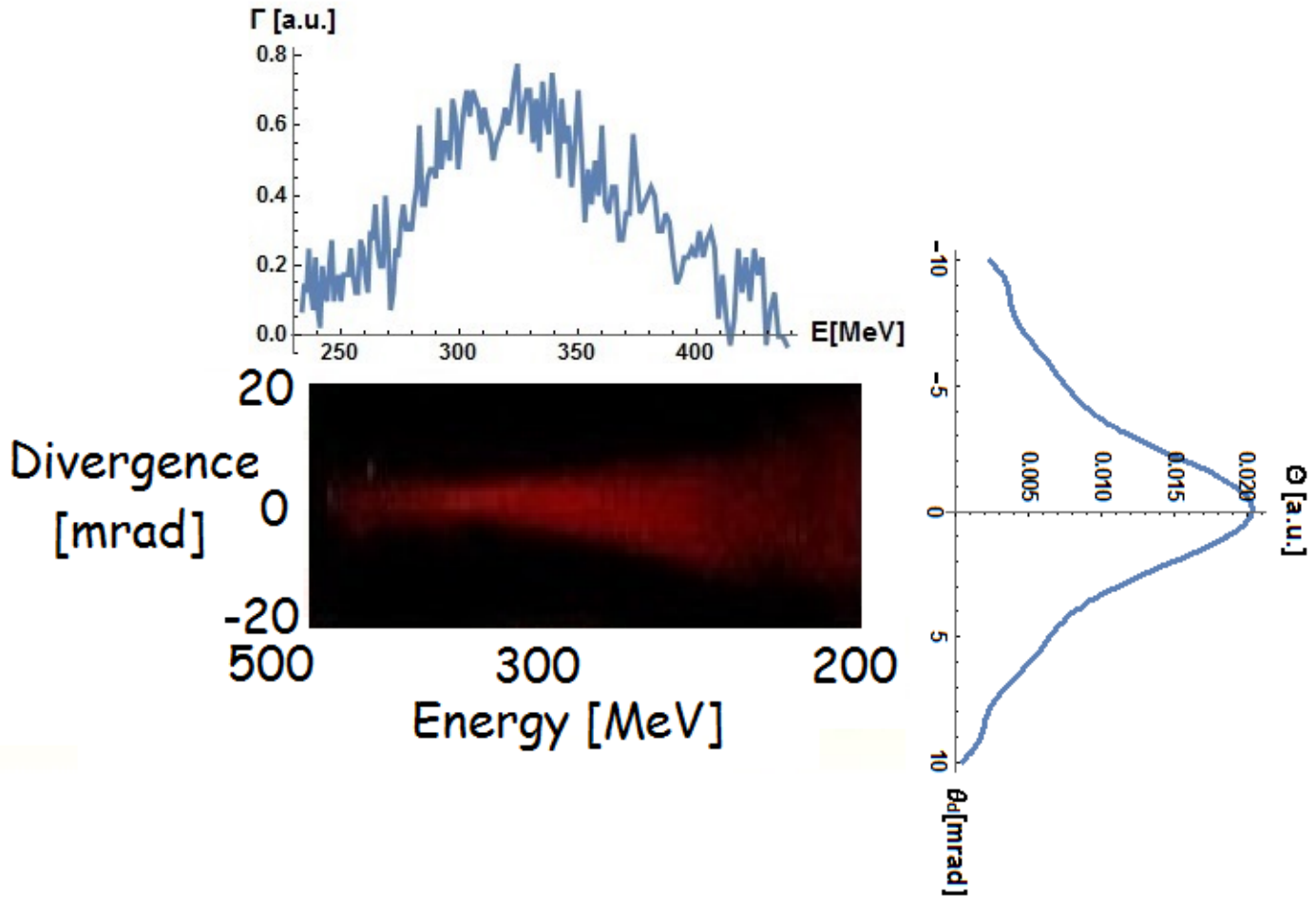

Figure: Electron energy spectrum relative to the electron bunch accelerated in the bubble regime. Central energy $\gamma_0 = 320\ MeV$, energy spread $2\sigma_\gamma/\gamma_0 \sim 20$ %. The outlines of the energy spectrum (up) and of the beam divergence (right) are reported.

Experimental Results: Beam Profile Reconstruction

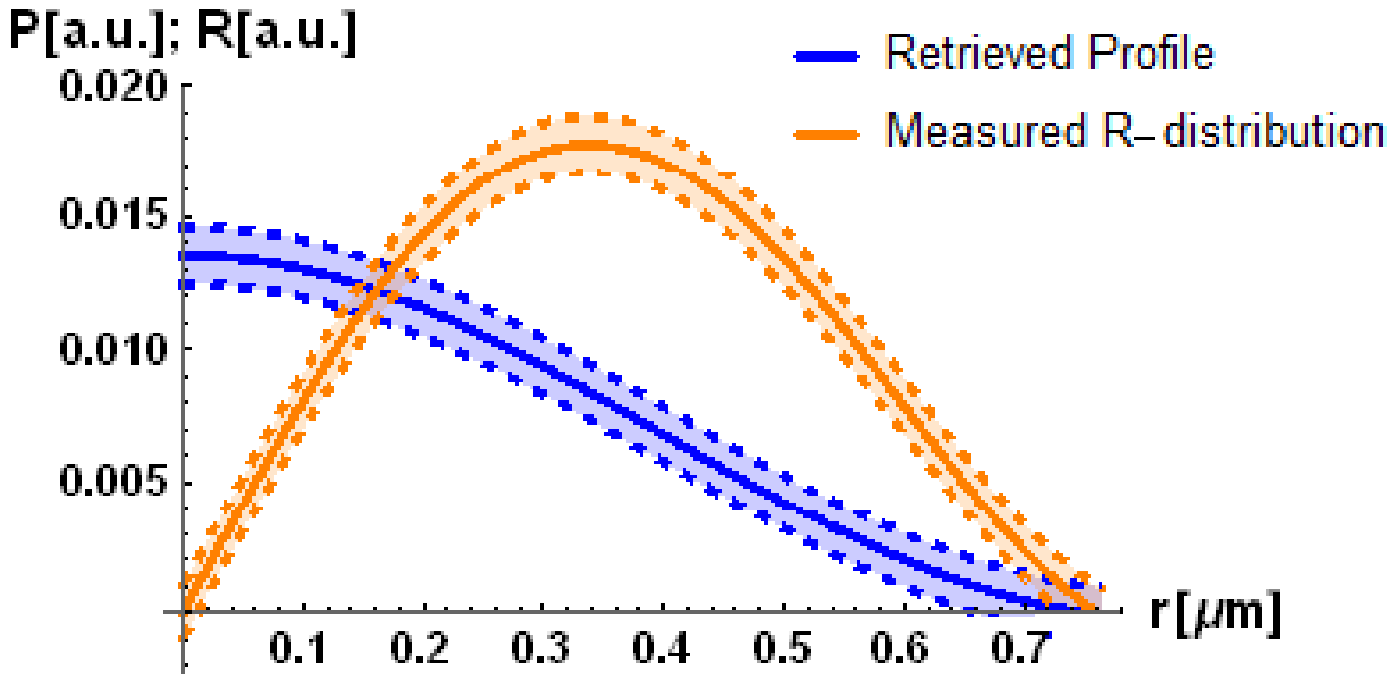

Figure: The beam profile $P(r)$ derived directly from the measured function $R(r_\beta)$. The rms betatron radius is found $\sigma_r \sim 0.42 \pm 0.04\ \mu m$.

Experimental Results: Radiation Beam Distribution

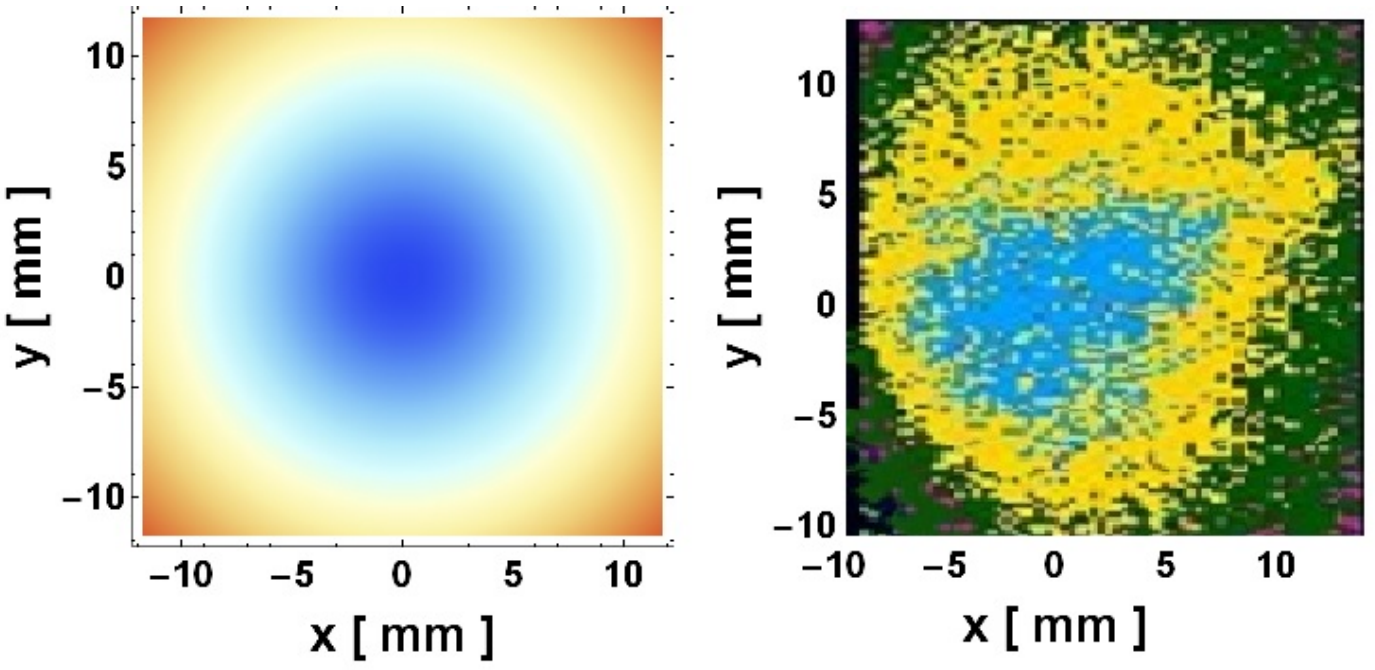

Figure: Betatron radiation spatial distribution: simulation (left) and measurement (right). Measured divergence of the radiation beam $\theta_\beta^{meas} = 8.2 \pm 0.3$ *mrad*, simulation value $\theta_\beta^{sim} = 8.5$ *mrad*.

Experimental Results: Distribution of the correlated divergences

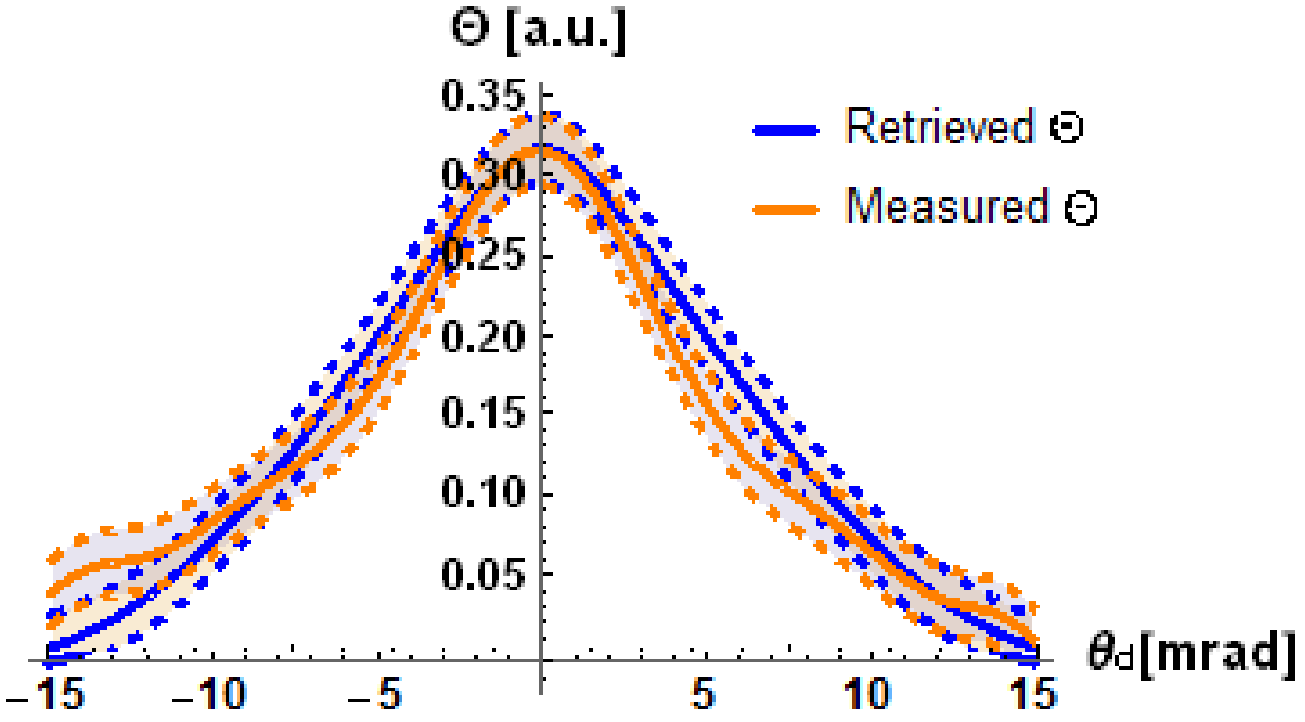

Figure: Comparison betweeen the measured and the retrieved $\Theta(\theta_d)$ function. Corresponding values of beam divergence $\sigma_\theta^{meas} = 5.9 \pm 0.6$ *mrad* and $\sigma_\theta^{retr} = 5.2 \pm 0.6$ *mrad*.

Experimental Results: Emittance Measurement

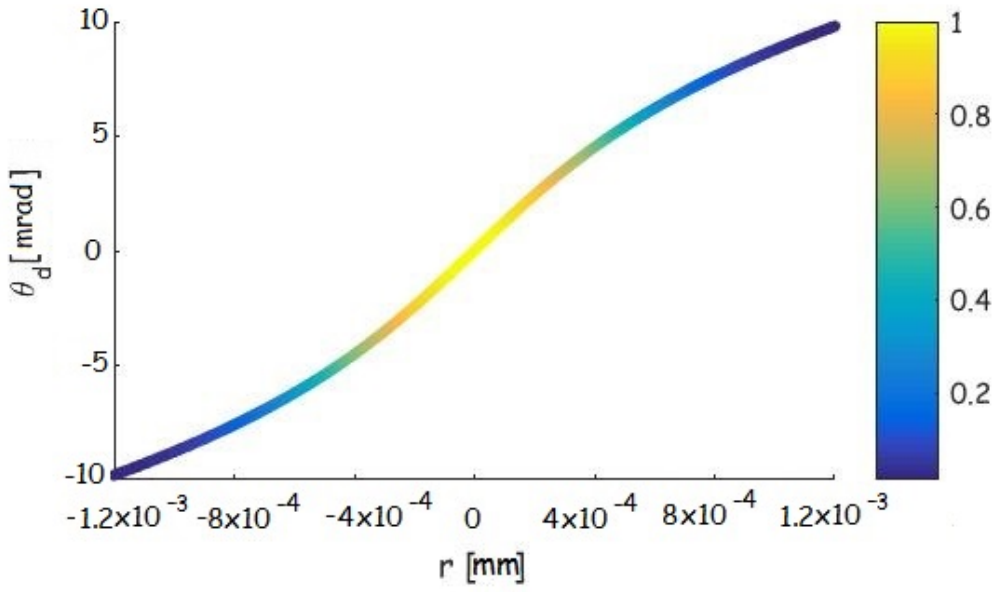

Figure: Reconstructed trace space density.

$$\epsilon_{r_\beta N} = \gamma_0 \sqrt{(\sigma_\gamma/\gamma_0)^2 \sigma_r^2 \sigma_\theta^2 + \epsilon_{r_\beta}^2} = (0.6 \pm 0.1)\ mm\ mrad$$

Upper Limit: $\gamma_0 \sigma_r \sigma_\theta^{meas} = (1.5 \pm 0.3)\ mm\ mrad$

Relativistic Self Focusing

⋆ *Curcio, A. et al. Ray optics hamiltonian approach to relativistic self focusing of ultraintense lasers in underdense plasmas. To be submitted to Optics Letters.*

Experimental Results: Plasma channel

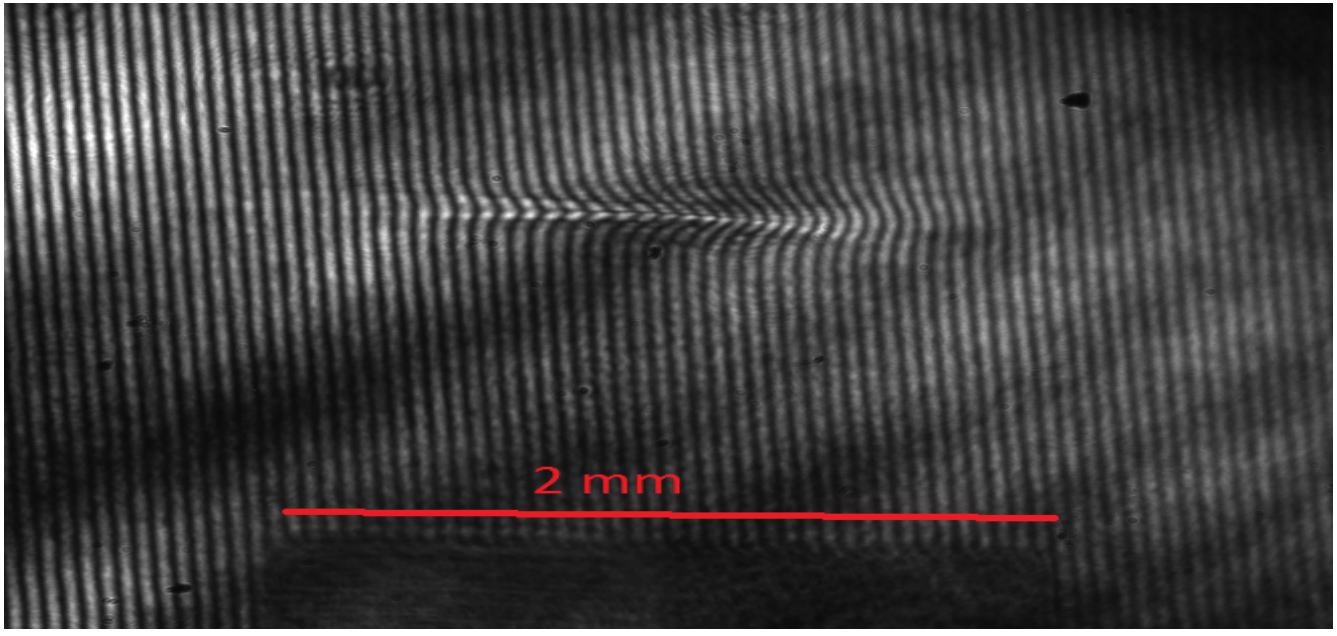

Figure: The Rayleigh length of the laser is evaluated $z_R \sim 100\ \mu m$, while the detected high-intensity/high-density ($8 \times 10^{18} cm^{-3}$) region, where the acceleration occurs, is longer than one millimeter.

Index of refraction $n \sim \sqrt{1 - \frac{\omega_p^2}{\gamma(a^2)\omega_0^2}}$

$a^2(x, y, z, t) \propto I(x, y, z, t)$ (Laser Intensity)

A hamiltonian approach to relativistic self focusing

$$H = -\sqrt{n^2 - p_r^2} \tag{1}$$

where p_r is the light ray radial momentum. The index of refraction is:

$$n = \sqrt{1 - \frac{\omega_p^2}{\gamma \omega_0^2}} \tag{2}$$

$$\frac{d\theta}{dz} \approx (1 + \theta^2)^2 \frac{d \log n}{dr} \tag{3}$$

The radial coordinate of the light ray as function of z comes directly from the integration of θ after solving the equation 3, namely:

$$r(z) = r_0 + \int_0^z \theta dz \tag{4}$$

where r_0 is the initial radial position of the light ray. Notice that equation 3 is analytically integrable, yielding the following result for θ:

$$\frac{1}{2}\left(\frac{\theta}{1 + \theta^2} + arctan\theta\right) = \theta_0 + \int_0^z \frac{d \log n}{dr} dz \tag{5}$$

where θ_0 is an integration constant. When considering for example a laser beam it is possible to define, once the radial distribution R(r) of the laser energy is known, the beam radius:

$$\sigma(z) = \sqrt{< r(z, r_0)^2 > - < r(z, r_0) >^2} \tag{6}$$

Numerical results

Channeling, ionizing and heating

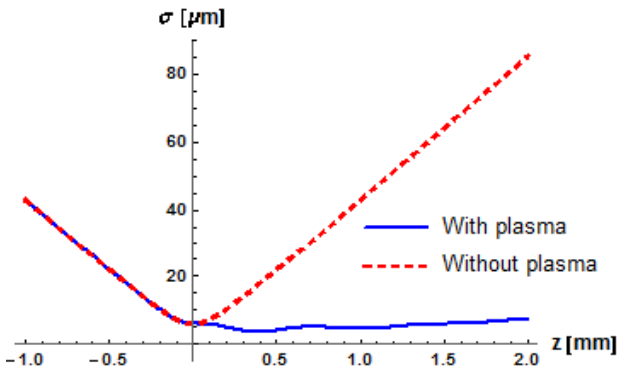

The comparison between the free propagation beam radius of the FLAME laser in vacuum (red) and the beam radius determined by the relativistic self focusing of FLAME propagating inside the He underdense plasma (blue). The zero point corresponds to the beginning of the plasma region ($z > 0$).

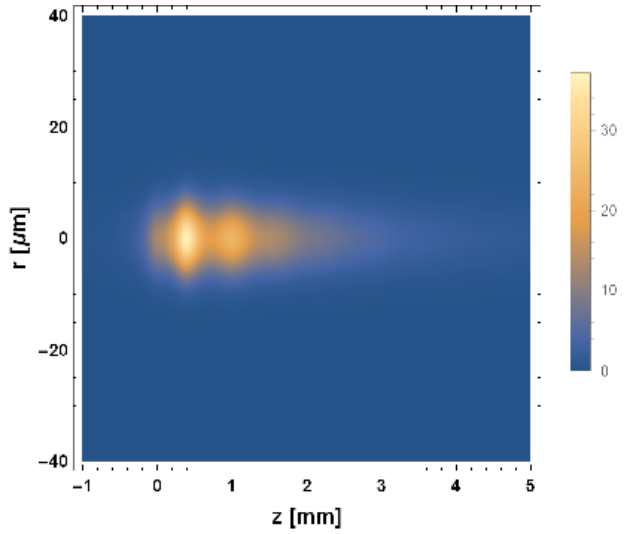

Normalized laser intensity a^2 of the laser FLAME propagating from left to the right from vacuum to the He gas-jet. The zero point corresponds to the beginning of the plasma region ($z > 0$).

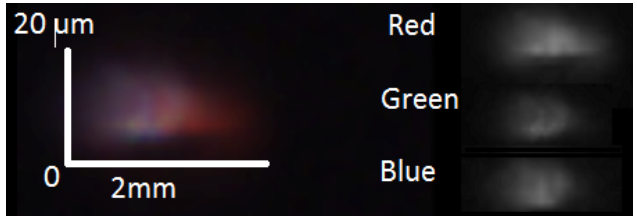

Picture of the plasma channel in RGB colors: red (570-750 nm), green (495-570 nm), blue (380-495 nm).

X-ray production from plasma filaments in front of solid targets

⋆ *Curcio, A. et al. Characterization of X-ray radiation from solid Sn target irradiated by femtosecond laser pulses in the presence of air plasma sparks. Laser and Particle Beams (2016), 34, 533538. Cambridge University Press, 2016 0263-0346/16 doi:10.1017/S026303461600045 8.*

Interaction of few TW laser with air-plasma filaments/1

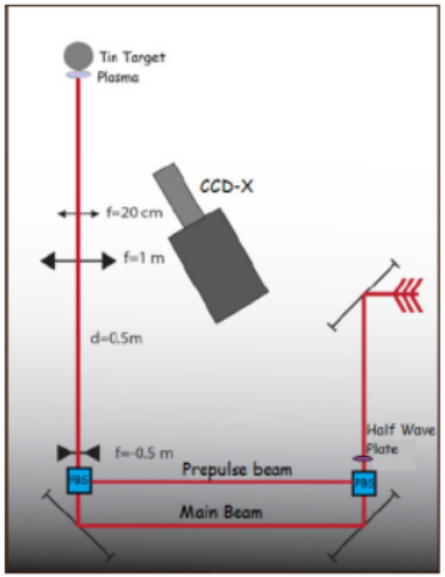

Experimental setup: the laser beam starts from the right, and then it passes through a half-wave plate in order to distribute the laser energy into the s and p polarizations in a controlled way. After this, the laser is split in polarization by a polarizing beam splitter. The delay line between the main pulse and the prepulse is 0.5 ns. A telescope is mounted with the goal to increase the beam diameter at the entrance of the last focusing lens. The two pulses are focused in air by a 20 cm positive lens. The air plasma is formed in front of the Sn target. When target is moved along the spark X-rays are observed and detected by a CCD-X in single-photon counting mode.

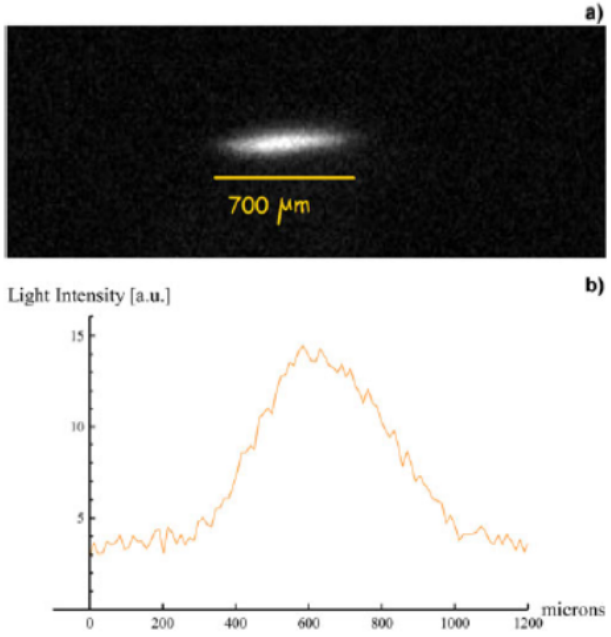

(a) Spectral and temporal integrated plasma light: longitudinal profile of the plasma spark. (b) Line-out of the longitudinal profile of the plasma spark.

Interaction of few TW laser with air-plasma filaments/2

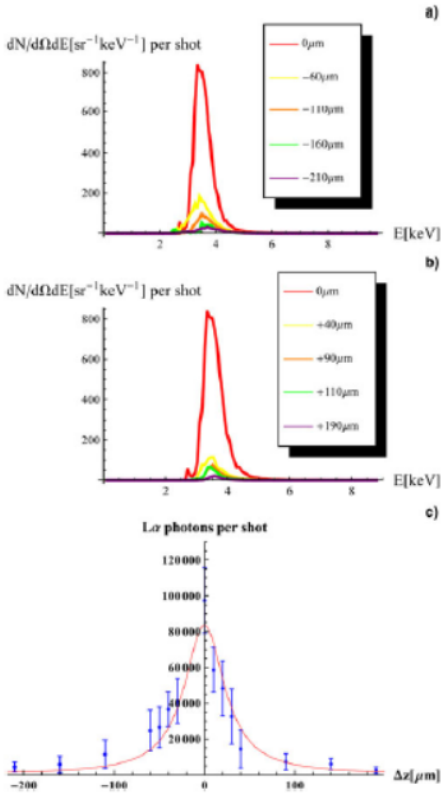

X-ray spectra for different negative (a, toward the incoming laser)/positive (b,in the same vs. of the incoming laser) positions of the Sn target inside the plasma channel with respect to the optimum point taken as the origin of the displacements. The optimum point is found in the center of the plasma spark. The optimum point is found in the center of the plasma spark. (c) Summary of the focus-scan results. FWHM width of the Lorentzian fit $\Delta z = 27\ \mu m$. The spectral and angular integrated number of L_α photons is reported with respect to the position of the target.

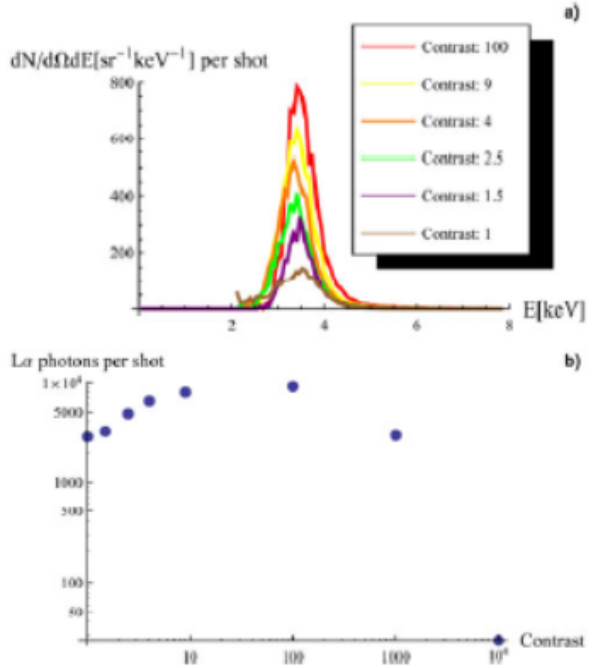

(a) X-ray spectra for different contrast value. The target is positioned in the optimum point for the yield L_α photons, and then with the help of the half-wave plate the energy ratio between the main pulse and the prepulse is adjusted. (b) Number of L photons versus laser contrast. The target is positioned in the optimum point for the yield L_α photons. The spectral and angular integrated number of L_α photons is reported with respect to the energy ratio (contrast) between the main pulse and the prepulse.

Self-phase modulation

⋆*Giulietti, D. and Curcio, A. Self-Phase Modulation Effects as Laser Produced Plasma Diagnostics. Journal of Instrumentation 11(08):C08011-C08011 August 2016 DOI: 10.1088/1748-0221/11/08/C08011*

Self-phase modulation as diagnostics

Laser phase

$$\phi = k_0 \int_0^z \mu(z,t)\, dz - \omega t$$

$$\omega = -\frac{d\phi}{dt}$$

$$\omega - \omega_0 = -k_0 \int_0^z \mu(z,t)\, dz$$

$$\frac{d\mu}{dt} > 0 \rightarrow red\ shift$$

$$\frac{d\mu}{dt} < 0 \rightarrow blue\ shift$$

Index of refraction

$$\mu = \sqrt{1 - \frac{\omega_p^2}{\gamma\omega^2}}$$

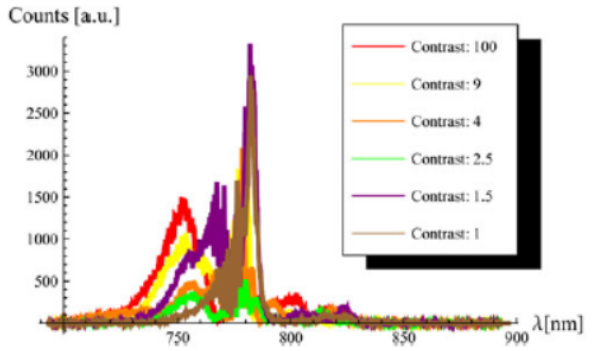

Near-infrared laser spectra at the exit of the plasma channel for different contrast values.

Laser-plasma interaction in capillary waveguides

⋆ *Curcio, A. et al. Numerical and analytical models to study the laser-driven plasma perturbation in a dielectric gas-filled capillary waveguide. Op. Lett. 41, 18; http://dx.doi.org/10.1364/OL.99.099999 (2016).*

Plasma channels in capillary waveguides/1

Propagation model:

$$\star\left[\frac{\partial^2}{c^2\partial t^2}-\frac{2}{c}\frac{\partial^2}{\partial\zeta\partial t}\right]c_n(\zeta,t)+\frac{1}{a_{n0}^2}\sum_m P_{nm}(\zeta,t)c_m(\zeta,t)=0$$

Plasma operator:

$$\star\frac{P_{nm}}{k_{p0}^2}=<a_n|\frac{1}{\gamma}+\frac{c^2}{2\gamma\omega_{p0}}\int_0^t dt'\sin[\omega_{p0}(t-t')]\nabla^2(\sum_n c_n a_n)^2|a_m>$$

Scalar product:

$$\star<a_n|\hat{P}|a_m>\sim 2a_{n0}a_{m0}\frac{\int_0^1 dx J_0(u_n x)x\hat{P}J_0(u_m x)}{J_1^2(u_m)}$$

Plasma channels in capillary waveguides/2

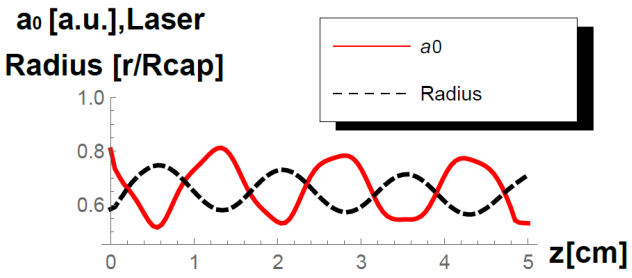

The normalized vector potential along the capillary axis and the laser beam radius normalized to the capillary radius.

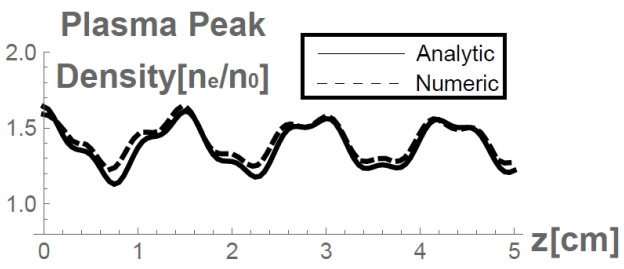

The comparison between the numerical model (dashed line) and the analytical model (continuous line).

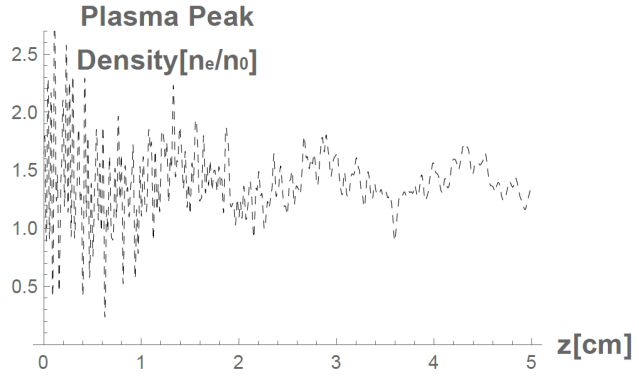

Electron plasma wave peak density along the capillary when the ionization is implemented by the ultra-short laser pulse itself.

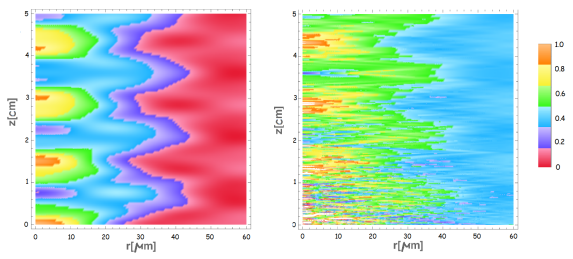

Laser intensity [a.u.] 2D map of a capillary guided pulse propagating through a preionized/non preionized (left/right) gas.

Tuning of betatron radiation with multimode propagation in waveguides

Laser mode matching

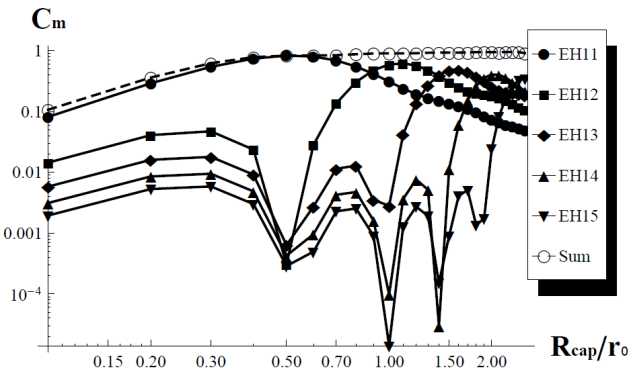

The coupling efficiency coefficients for a flat top profile laser focused into a dielectric capillary tube.

⋆ *Curcio, A. et al. Tuning of Betatron Radiation in Laser-Plasma Accelerators via Multimodal Laser Propagation through Capillary Waveguides. To be submitted to Physics of Plasmas.*

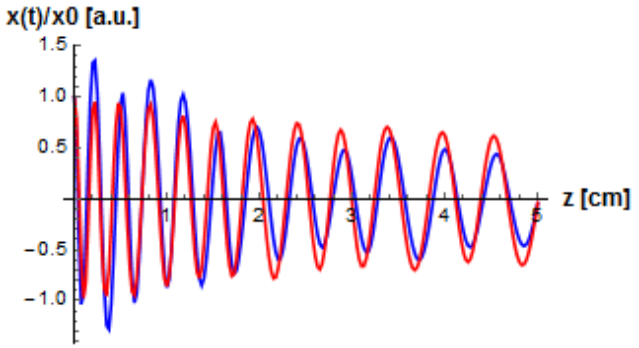

Betatron oscillations for a single test electron along the capillary. First configuration (red) for the initial laser matching into the capillary: $R_{cap}/r_0 = 0.5$. Second configuration (blue): $R_{cap}/r_0 = 4$.

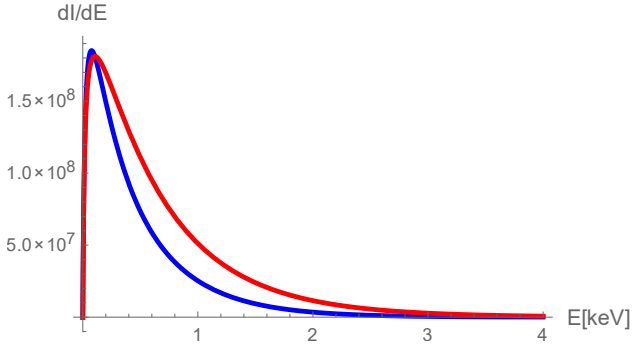

Spectrum comparison between the first (red) and the second configuration (blue) ($R_{cap}/r_0 = 0.5$ and $R_{cap}/r_0 = 2$). The spectrum in the second configuration is tuned towards higher photon energies.

Resonant betatron oscillations

⋆ *Curcio, A. et al. Resonant interaction between laser and electrons undergoing betatron oscillations in the bubble regime. J. Plasma Phys. (2015), vol. 81, 495810513 c Cambridge University Press 2015 doi:10.1017/S0022377815000926*

Laser-driven resonant betatron oscillations/1

$$x(t) \sim A\,P_v(\tau) + B\,Q_v(\tau) + \frac{6eE_0}{a_0\left|\frac{a_0}{3}-1\right| m\omega_p^2}\exp\left(\frac{(z(t)-2R-v_g t)^2}{2v_g^2\Delta\tau^2}\right)\cos\sqrt{\frac{a_0}{3}}\omega_\beta t,$$

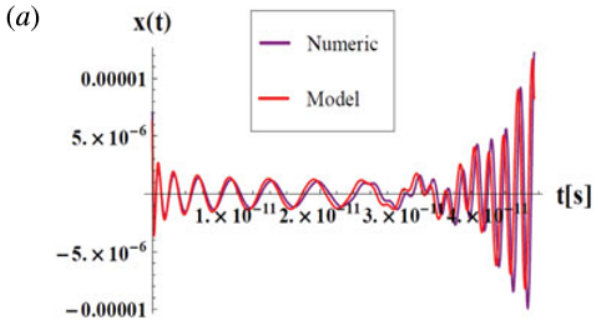

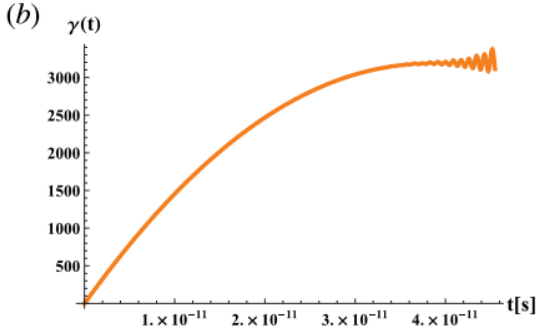

(a) Comparison between numerical and analytical results for the transverse dynamics of an electron undergoing laser-driven betatron oscillations near the dephasing point in the bubble regime. Electron plasma density $n_e = 1.8 \times 10^{18} cm^{-3}$, laser intensity $I_0 = 4.7 \times 10^{19} W/cm^2$. The laser-driven oscillatory motion develops preferentially on the third harmonic of the betatron frequency, i.e. during the major part of the laserelectron interaction time; the driving frequency of the laser ω_s is witnessed by the accelerated electrons as $3\omega_\beta$. (b) Electron energy as a function of time.

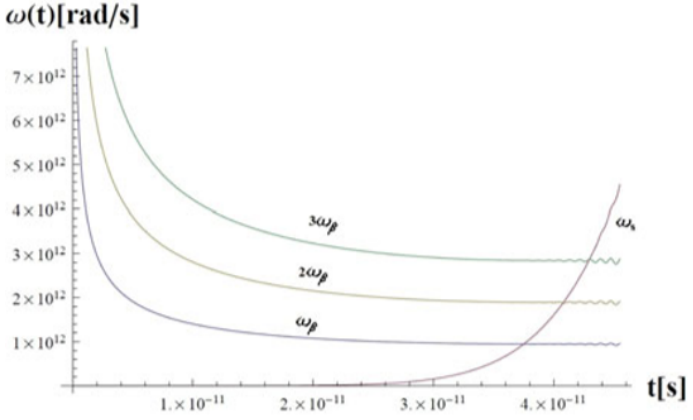

Laser frequency as witnessed by the electrons ω_s.

Laser-driven resonant betatron oscillations/2

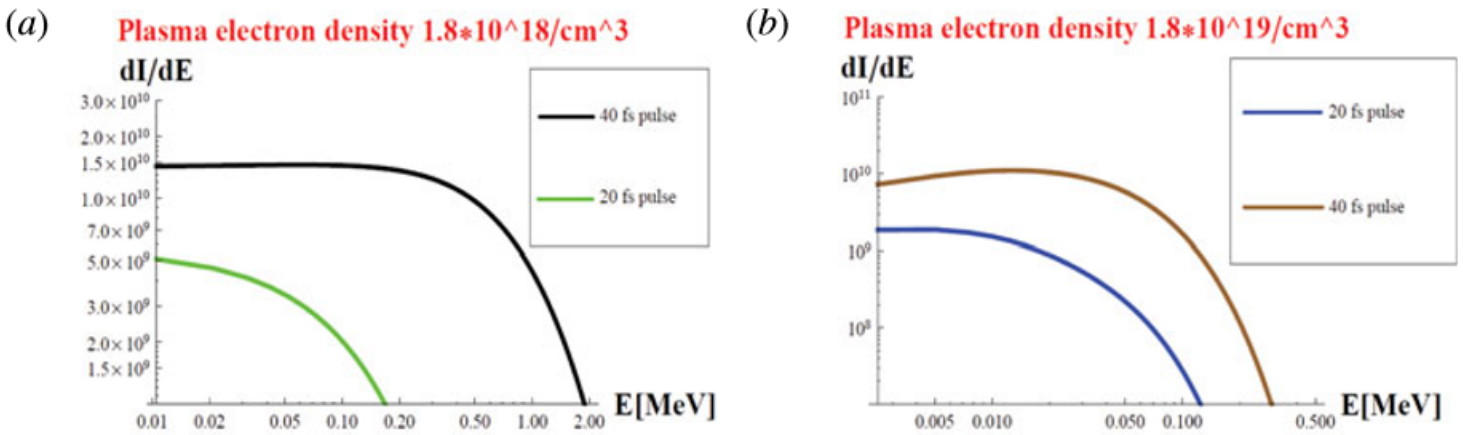

Spectra of the radiated energy dI per energy interval dE. Laser pulse energy 6 J, electron bunch charge Q = 100 pC, diameter of the laser focal spot 10 μ m. (a) Comparison between betatron spectra emitted by accelerated electrons ($\gamma_{max} = 4200$) in a plasma bubble with density $n_e = 1.8 \times 10^{18} cm^{-3}$ at different laser pulse durations, respectively 40 fs (black curve) and 20 fs (green curve). Acceleration length 11 mm. (b) Comparison between betatron spectra emitted by accelerated electrons ($\gamma_{max} = 3200$) in a plasma bubble with density $n_e = 1.8 \times 10^{19} cm^{-3}$at different laser pulse durations, respectively 40 fs (brown curve) and 20 fs (blue curve). Acceleration length 570 μm.

Laser-driven resonant betatron oscillations/3

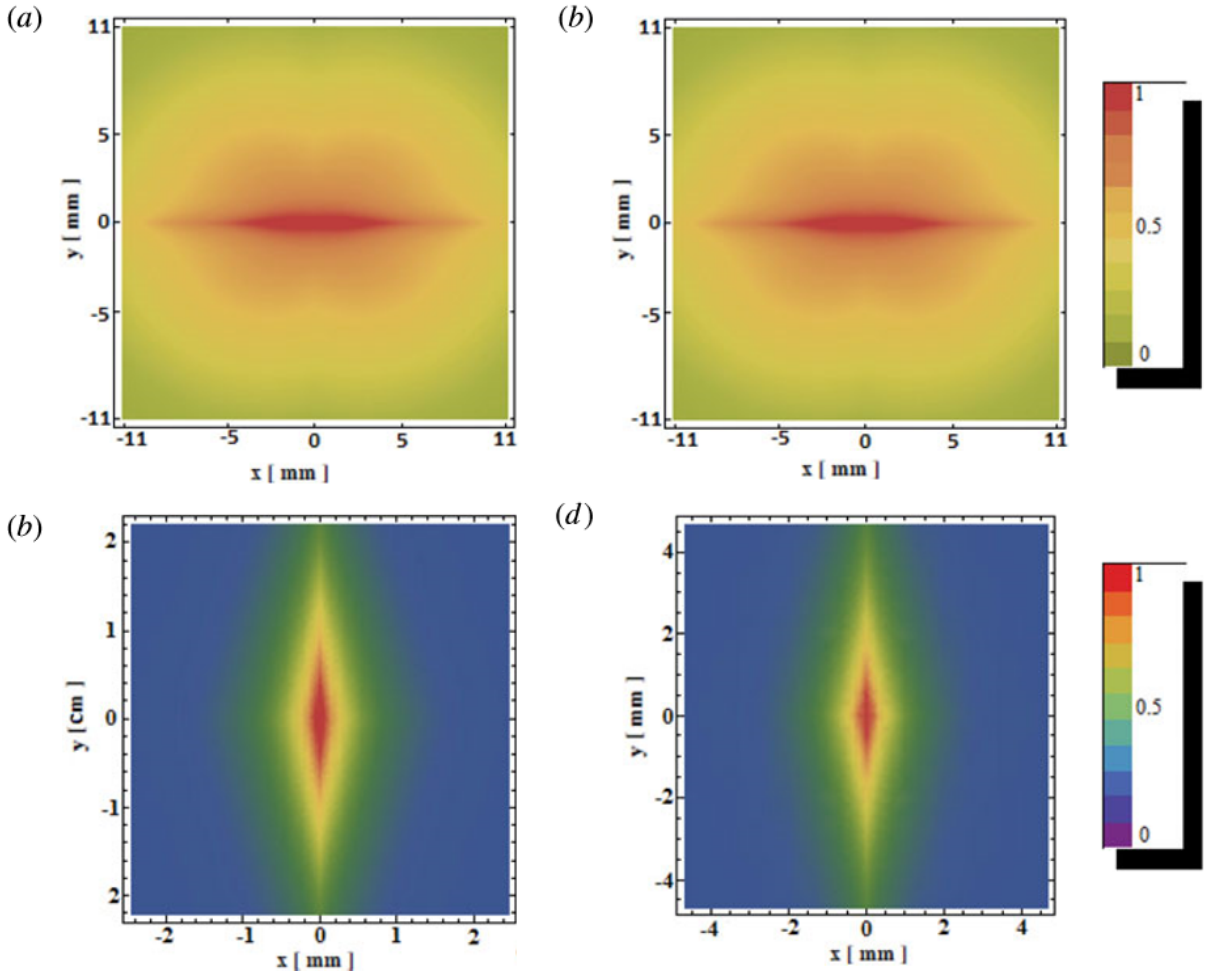

Spatial distribution of the radiation collected at 1 m from the interaction region. Laser pulse energy 6 J, electron bunch charge Q = 100 pC, diameter of the laser focal spot 10 μm. (a) Red indicates 7 μJ/ mm^2, laser pulse duration 40 fs, laser polarization along x, electron plasma density $n_e = 1.8 \times 10^{18} cm^{-3}$. (b) Red indicates 0.5 μJ/mm^2, laser pulse duration 20 fs, laser polarization along x, electron plasma density $n_e = 1.8 \times 10^{18} cm^{-3}$. (c) Red indicates 160 μJ/mm^2, laser pulse duration 40 fs, laser polarization along y, electron plasma density $n_e = 1.8 \times 10^{19} cm^{-3}$. (d) Red indicates 10 μJ mm^2, laser pulse duration 20 fs, laser polarization along y, electron plasma density $n_e = 1.8 \times 10^{19} cm^{-3}$.

Thanks for your attention